# Understanding the influence of laminate stacking sequence on strain/stress concentrations in thin laminates at repair holes with large scarf angles

Mahdi Damghani[1], Jerzy Bakunowicz[1] and Adrian Murphy[2]

[1] *Department of Engineering Design and Mathematics, University of the West of England (UWE), Bristol, BS16 1QY, UK*

[2] *School of Mechanical & Aerospace Engineering, Queen's University Belfast, Ashby Building, Stranmillis Road, Belfast. BT9 5AH*

**Abstract**

Scarf repair is widely used in the restoration of structural performance of damaged aircraft secondary structure. Such repairs result in reduced thickness sections which are significantly larger than those associated with typical fastener holes. Significant literature exists on the distribution of strain/stress concentration in fastener hole geometries, both straight sided and countersunk, but is lacking for the geometries associated with shallow scarf angles and thin laminates. Hence, herein three-dimensional finite element models are developed to understand the influence of stacking sequence and scarf angle on strain/stress concentrations. The results demonstrate and quantify for the first time that strain concentrations are not only dependant on the laminate membrane stiffness but also on laminate bending stiffness, due to the anisotropy created as a result of scarfing angle, hole geometry and laminate thickness. Scarfing is demonstrated, for typical repair geometry associated with foreign object damage (hole diameter 20 mm, scarf angles 3º to 7º), to elevate strains by up to 2.5 times when compared to equivalent diameter straight sided holes in laminates of thickness ≈ 1 mm.

**Keyword:** Scarf repair, scarf holes, scarf angle, stacking sequence, strain concentrations, stress concentrations, composite laminate.

# 1    Introduction

Carbon fibre reinforced polymer (CFRP) composites have become the material of choice for a significant volume of the structure of an aircraft. CFRP materials have for many years been used for the primary structures of light aeroplanes, gliders and military aircraft. Only in recent years with the advent of civil transport aircraft such as the Boeing 787, the Airbus A350 XWB and A220 the application of CFRP materials in civilian aircraft has evolved from secondary structures such as fairings to primary and load bearing structures such as the wing box and fuselage (1,2). A significant difference between light aeroplanes and large airliners is the change from a monocoque to a stressed-skin construction, enabling high levels of structural loading and structural efficiency (3). The primary differences between a military and civilian aircraft can be the service loads, service duration and the required ratio of flight to maintenance hours. CFRP materials are known to provide superior performance with regard to their specific strength and stiffness but importantly are also resistant to fatigue and corrosion. However, the laminated nature of the material combined with the typical thermoset polymers used means they are sensitive to defects and impact damage and maintenance and repair needs to be a critical design consideration.

Significant knowledge and knowhow exists for design and structural analysis of CFRP materials. However, limited experience and data is currently available for the maintenance and repair of such structures in civilian aircraft operations. The noteworthy design and use differences between large civilian aircraft and light aeroplanes, gliders and military aircraft means significant effort is ongoing to understand CFRP materials in this new service environment. This paper focuses on the structural impact of the restoration processes for damaged or defective CFRP material where material is removed in a greater volume than required in manufacturing for the installation of mechanical fasteners. In particular, this paper

examines the impact of shallow scarf angles and the resulting influence on strain and stress distributions, which ultimately influence the strength performance of the repaired structure.

## 2    Background

During the production of CFRP components defects are possible in the form of inclusions, voids and weak bonding. CFRP structures will also be subjected to accidental damage during manufacture and throughout their life, from tool drop to collision with ground equipment. Significant inflight damage may also take place due to lightning and bird strike. If the defects or damage has weakened the structure through fibre fracture, delamination or dis-bonding, the repair will involve replacement of the damaged fibre reinforcement to restore the original mechanical properties, i.e. stiffness, strength and durability (4).

Structural repairs can be achieved via mechanical fastening (4,5), adhesive bonding (6,7) and hybrid fastening and bonding (8). Considering the advances in manufacturing processes (9), bonded repairs to primary or flight-critical components are becoming a reality. They are desirable as they do not require mechanical fasteners resulting in a lighter repair scheme. At present, there are three adhesive bonding repair schemes being implemented for aerospace structures, i.e. patch repair (one-sided or double-sided), taper sanded (scarf) repair and stepped sanded repair (10). Each of these schemes has its advantages and disadvantages. Repair patch schemes, whether one-sided or double-sided, are fast to apply, however, they disturb aerodynamic behaviour of the surface they are going to be applied to and add undue extra weight to the structure (11). Tapered scarf repairs can restore up to 93% of the strength of unflawed composite laminate (1,11). However, the repair efficiency of scarf repairs is dependent upon their manufacturing process, scarf angle and are time consuming to apply. For instance, water jet machining or drilling could be employed for scarfing of composite structures in service, however, such processes could impose stresses and cracks and hence damaging the

laminate to be repaired, leading to reduction of overall static and fatigue strength of the structure (12,13). Such damage could be significant to the extent of 30% reduction in tensile strength of the laminate (13). Both experimental and finite element analysis (FEA) have demonstrated repair efficiency of 80% and above with shallow scarf angles ranging from 2º to 7º (14–16). In general scarf repairs have better aerodynamic performance, introduce no load eccentricity, have better aesthetic and do not reduce resale aircraft value adversely compared to patch and mechanically fastened schemes. Thus scarf repairs are currently used for aircraft secondary structures.

There are numerous research works on scarf repaired composites in the literature addressing repair parameters such as repair patch shape, scarf angle, repair patch stacking sequence, bond-line adhesive material, with each typically assessing the overall strength of the repaired laminate. For example, Wang et al. (17) presented an optimisation study of the ideal shapes of scarf repairs to orthotropic composite laminates subjected to biaxial stresses. They developed a shape optimisation strategy to take account of the non-uniformity of the stresses along the scarf bond-line and enforcing the average shear stress in the adhesive to remain constant. They proposed that the optimum repair shape for low scarf angles is concentric ellipse with the aspect ratio being approximately equal to the biaxial stress ratio and a hybrid square-ellipse profile for high aspect ratio damage. Riccio et al. (18) proposed an elasto-plastic material model for the failure behaviour of structural ductile adhesives. They demonstrated a good correlation between the numerical results obtained with the proposed novel material model and preceding simulation and experimental results from literature. Bendemra et al. (19) carried out extensive numerical investigation and parametric study of the influence of joint parameters including scarf angle and stacking sequence on peak stresses in the adhesive bond-line in tapered scarf and stepped-lap repairs. Amongst the highlights of their study was the importance of the 0º plies location in the composite laminates. Indeed, the adhesive region

adjacent to the 0º plies were prone to develop stress concentration as the majority of the load transfer, when loaded under tension, occurred at the location near the stiffer plies.

Despite the developed knowledge on the design, modelling and strength behaviour of repairs, from an airworthiness stand point, a prepared/scarfed CFRP structure needs to withstand the aircraft limit loads assuming the patch has become structurally ineffective. This requirement is to ensure flight safety in the occurrence of a repair patch becoming detached during operations due to some unforeseen events (20). Therefore, it is necessary to understand strain/stress concentrations around scarfed holes. This is due to the fact that areas of high strain/stress concentration are potential areas of damage initiation and propagation. Geometric features, such as scarfed holes, will have a negative impact under tension loading as a result of their inability to redistribute stresses in the vicinity of the feature leading to earlier brittle material failure (21).

Although strain/stress concentration around straight sided holes in both isotropic and orthotropic plates has been extensively studied in the literature (22–27), the amount of literature on scarfed holes in orthotropic composite laminates is very scarce. Amongst such few studies is the work of Wang et al. (20). In the investigation, the progression of damage initiated from scarfed circular/elliptical holes were studied and compared with straight sided holes. Experimental, numerical and analytical approaches demonstrated that in a CFRP laminate significantly higher strain concentration exists around a scarfed hole compared with a straight sided hole. It was concluded that due to the catastrophic nature of failure of the scarfed laminates, initiation and post initiation damage has little effect on laminate strength. However, their study was limited to only one scarf angle, i.e. 3º, and their assumption of strain distribution in the scarfed region, as will be shown later in this paper, was flawed.

Darwish et al. (28,29) carried out numerous FEA studies on orthotropic plates having countersunk holes. In the investigation the effect of countersunk size, plate thickness, and plate dimensions were investigated. Using factorial analysis, an equation was established by which the stress concentration factor for a countersunk hole could be related to a straight sided hole. Although their proposed model fits reasonably well with the presented numerical predictions, it cannot be directly applied to other problems and does not present a generic understanding on the influence of geometry and laminate stacking sequence on strain/stress concentration.

Given the limited literature, the goal of this study is to develop and provide a generic understanding of the strain/stress concentration phenomenon associated with shallow scarf angles in composite laminates using validated and calibrated numerical methods. This is due to the fact that, numerous literatures such as (26, 30–33) demonstrate the accuracy and efficiency of using detailed FEA for the prediction of stress/strain concentration in laminated composite structures. This includes an establish track record of prediction correlation with experimental work. Moreover, FEA is an appropriate method given the maturity and robustness of the technique in available commercial software, and its well-established ability to deal with problems with complex or varying geometry and orthotropic laminate materials. To this end, a number of objectives are defined which are addressed in the subsequent sections:

- provide an in depth and critical assessment of existing methods for approximation of strain/stress concentration in scarfed composite laminates (section 3);
- create a FEM modelling strategy which can be used to develop understanding on the influence of geometry and laminate stacking sequence on strain/stress concentration and verify the approach using well-established analytical solutions (section 4);

- complete a comprehensive modelling investigation to create a generic understanding of the strain/stress concentration phenomenon associated with shallow scarf angles in composite laminates (section 5).

## 3    Existing methods

As noted earlier, the amount of work on understanding stress/strain concentrations in scarfed composite laminates is very limited. As described previously, Darawish et al. (28,29) is one of a few researchers to study stress concentrations (Figure 1a). Darawish et al. concluded that a stress concentration factor in an orthotropic composite laminate may be expressed using Equation 1, where non-dimensional parameters $K_{h,o}$, $K_{ss,o}$, $K_{Cs,o}$ and $K_{\theta c,o}$ account for the effects of the width of plate, the thickness, the countersunk depth and the countersunk angle, respectively.

$$K_t = K_{h,o} \times K_{ss,o} \times K_{Cs,o} \times K_{\theta c,o} \tag{1}$$

Although the method provided in (28) was successfully applied to small holes (of the order of a typical aerospace fastener with diameter 6.41 mm and countersunk angle of 45°), for shallow scarf angles significant coupling effects are possible and an alternative modelling approach is required.  A greater scarf angle results in greater material removal and thinner more compliant laminates over greater areas. In fact, the finite element modelling work used quarter symmetry (Figure 1b), recreated herein to ensure modelling consistency. Such a modelling approach is not suitable for shallow scarf angles as the un-symmetric lay-up in the scarfed region may lead to potentially important bending-stretching coupling. In fact, the boundary conditions required for a quarter FEM constrains the structure to displace/rotate due to coupling effects hence overestimating strain values compared to that of full scarf models. To quantify this effect, two initial simulations were undertaken by the authors, the details of the modelling

approach are presented in the following section, and the boundary conditions and the results summarised in Figure 2a-c. This figure illustrates that for a scarfed hole of diameter 20 mm, the 3D quarter FEM idealisation results in strains which are 156% higher than those predicted by the full 3D FEM idealisation.

Other studies (20) suggest that the distribution of the hoop strain in scarfed laminates can be described in the same fashion as that for a circular straight hole. It is believed that the influence of tapering in the scarf causes a proportional increase in the hoop strain, which may be described by Equation (2). In the equation, $t$ $(=y-R)$ denote the distance away from the hole edge, where $E$ signifies the homogenised membrane stiffness of the composite laminate in the load carrying direction, i.e. $E_x$ in this study. $\sigma_n$ and $R$ are remote stress and radius of the hole, respectively.

$$\varepsilon_{\theta\theta} = \frac{K_t}{3}\left(1+\frac{1}{2}\frac{1}{\left(1+t/R\right)^2}+\frac{3}{2}\frac{1}{\left(1+t/R\right)^4}\right)\frac{\sigma_n}{E} \qquad (2)$$

To assess such an assumption for a shallow scarf angle Figure 3 illustrates the strain distribution from the edge of the hole for two laminate types, i.e. quasi-isotropic and hard laminates (again full details of the models are presented in the following section). Comparing the predictions from both the FEA method and using the published analytical solution (Equation (2))- it is evident in Figure 3 that such an analytical solution, intended for straight sided holes, may not be used for scarfed holes. For example, for quasi-isotropic laminates (see Figure 3a), the strain distribution is underestimated by the analytical solution. However, for the harder laminates (such as Figure 3b) the analytical solution generally overestimates the strain. It should be noted that the source of strain fluctuation in the FEA predictions (Figure 3) results from averaging nodal results through the thickness of the 3D model.

Moreover, in order to obtain resultant hoop stresses, changing sectional thickness in the scarfed region must be included. Based on the literature (3,20), the resultant hoop stress at a distance $t$ ahead of the hole edge can be approximated by Equation (3).

$$\sigma_{\theta\theta} = \frac{t\tan\alpha}{h} E_x(t)\varepsilon_{\theta\theta}(t) \tag{3}$$

Such an assumption is based on the linear distribution of the homogenised modulus of elasticity in the scarf region. However, this is not valid as the distribution of $E_x$ is nonlinear across a scarfed region, illustrated in Figure 4, and again generated by way of a FEA simulation (Section 4). The linear distribution assumption severely underestimates the stiffness in the immediate vicinity of the hole. The discrepancy between the assumed and actual stiffness distribution is dependent upon the stacking sequence and the scarf angle ($\alpha$) of the composite laminate. The use and development of analytical solutions such as Airy's stress functions that are suited for 2D plane strain/stress problems are limited for scarfed holes with shallow angles as a result of the coupling effects within the scarfed region.

In summary, the preceding work does not appropriately address scarfed holes associated with manufacturing or in-service repair. Many of the noted limitations may be addressed using a validated numerical FEA approach. Such modelling would allow new understanding to be obtained on the influence of scarfed holes on stress/strain concentrations in laminated composite structures. Moreover, such an approach would enable the development of repair design data, permitting iteration through various stacking sequences, limiting the need for significant volumes of experimental test. To this end the following section presents a FEA modelling method to appropriately represent a scarfed hole repair scheme to remove the constraints of the currently available solutions.

## 4    Numerical idealisation

A series of 3D Finite Element Models (FEM) of composite laminate structures with defined scarf angles were constructed using ABAQUS. Four models where initially built, three with angles which may be considered as shallow (3º, 5º, 7º) and a reference straight sided hole model (with a 90º scarf angle). As discussed in the preceding section, the use of computationally efficient quarter FEMs is not possible. Moreover, 2D modelling in which the scarfed region is modelled as stepped section properties is also not suitable, as such models do not accurately represent in detail the local behaviour at the change of thickness.

A square laminate structure is modelled of dimensions 250 mm × 250 mm having a central circular hole of diameter 20 mm. This arrangement gives a hole diameter to specimen global width ratio of 12.5. This ratio was selected to represent an infinite plate condition with a minimal edge effect on strain and stress values. The selected ratio ensures a homogenous strain distribution at the model edge, being greater than 3 radii from the modelled whole edge. The hole size is chosen to represent a typical damage size as the result of foreign object damage. It is assumed that the structure is comprised of 8 unidirectional plies through the thickness with mechanical properties as given in Table 1. The choice of 8 plies was adopted to not only cover a wide spectrum of laminate homogenised stiffness values but also reduce computational effort for a full parametric study. The orientation of each ply is arranged to give a balanced and symmetric lay-up covering a wide spectrum of homogenised modulus of elasticity in $x$ and $y$ directions as well as homogenised shear modulus (ranging between 5.58-30.63 MPa) in $xy$ plane. Moreover, the generated stacking sequences includes purely angle-plies, quasi-isotropic (25%/50%/25% for plies 0/45/90), soft (10%/80%/10% for plies 0/45/90) and hard (40%/20%/40% for plies 0/45/90) laminates. It is worth noting that soft and hard laminates are often used for spar and skin components, respectively, and thus it is appropriate to study both. This enabled the study of 46 different stacking sequences as given in Table A-1 of the appendix.

Two C3D8 (eight node linear brick elements) elements are used through the thickness to represent each ply. Therefore, 16 elements represent the total thickness of the laminate as shown in Figure 5. Boundary conditions and loading are designed to duplicate that of a uniaxial tensile test. Hence, one end of the structure is assumed to be fully clamped, i.e. constrained from rotating about $x$, $y$ and $z$ axes and displacing in $x$, $y$ and $z$ directions. However, the loaded end of the structure is constrained from rotating about $x$, $y$ and $z$ axes and displacing in $y$ and $z$ directions. A concentrated uniaxial tensile load of 37,500N is applied at a reference point which is kinematically constrained to the loaded surface. This arrangement produces a 100MPa of average tensile stress on the loaded end. The other two edges are considered to be free.

In the absence of experimental procedures, it is essential to verify the modelling strategy of the numerical method. Hence, a comparison of the predicted strain concentration value for a selected stacking sequence, [45/-45/0/90]s, was performed for a straight sided hole against available analytical solutions given in (24,26). It is worth noting that the analytical solution has been validated against both experimental and numerical procedures in various literatures such as Taboul et al. (34) and Hufenbach et al. (31). The 2D analytical equation for stress resultant/strain concentration ($K_t$) in an infinite thin orthotropic plate with a central straight sided hole is given by Equation (4).

$$K_t = 1 + \sqrt{2\left[\sqrt{\frac{E_x}{E_y}} - \upsilon_{xy} + \frac{E_x}{2G_{xy}}\right]} \tag{4}$$

This yields an analytical solution of $K_t = 3$ for the selected stacking sequence. As shown in Figure 6, the numerical model yields a maximum strain of 0.006336 and a remote strain of 0.002154 giving a numerical solution of $K_t = 0.006336/0.002154 = 2.94$. This is in close agreement with the analytical solution. Furthermore, a mesh sensitivity analysis was performed

(Figure 7) on the most shallow scarf angle, i.e. 3°, and 120 elements around the hole were determined to provide appropriate accuracy for strain prediction.

## 5    Results and Discussion

Matching the verification process and to aid in creating easily interpretable generic results concentration factors will be calculated from each simulation result. The maximum predicted strain around the hole ($\varepsilon_{max}$) is thus divided by the matching remote strain ($\varepsilon_n$) value to give a strain concentration factor, henceforth denoted as STRCF (Equation 5).

$$STRCF = \frac{\varepsilon_{max}}{\varepsilon_n} \tag{5}$$

Although the location with the highest STRCF is always at the edge of the hole (on the scarfed surface), this cannot be concluded for the determination of the stress concentration factor, henceforth denoted as SCF. For this, the distribution of STRCF along the scarf is required. Often, plies that make the smallest angle with the loading direction, i.e. 0° plies, have the highest SCF as they carry most of the load when compared with the off axis plies. Therefore, in order to obtain SCF in scarfed composites, the distribution of strain is crucial with SCF calculated using Equation 6. In which $E_{xp_i}$ and $\sigma_n$ are the modulus of elasticity of ply $i$ in the loading direction and remote stress, respectively.

$$SCF = K_t = \max\left(\frac{E_{xp_i}\varepsilon_{\theta\theta}}{\sigma_n}\right) \tag{6}$$

Figure 8 presents the values of STRCF against $E_x / E_y$ ratio for various homogenised values of $G_{xy}$ (see Table A-1). It is evident that all scarf angles, i.e. 3°, 5° and 7° (Figure 8a-c), are demonstrating similar qualitative behaviour comparable to that of a straight sided hole (Figure 8d). In other words, as it is expected from Equation (4) and numerical results show, a

higher ratio of $E_x / E_y$ leads to higher SCF and STRCF for all test cases and scarf angles. Moreover, laminates with higher $G_{xy}$ have lower SCF and STRCF although this is mostly dependant on the ratio of $E_x / G_{xy}$ rather than solely $G_{xy}$, as can be inferred from Equation (4). It is worth noting that in Figure 8 and for all test cases, the existence of several data points for laminates of equal $E_x / E_y$ ratio and $G_{xy}$ is associated to Poisson ratio effects ($v_{xy}$) for straight sided holes resulting from different stacking sequences. This can be inferred from Equation (4). However, the difference between STRCF of such laminates is significantly higher at a scarfed hole than witnessed at a straight sided hole. A contributory factor to Poisson ratio effects is bending, bending-stretching coupling and anisotropy in the scarfed region.

On the other hand, quantitative comparison of strain concentration suggests that STRCF increases with the decrease of scarf angle for the same $E_x / E_y$ and $G_{xy}$. For example, STRCF values for $E_x / E_y = 1$ and $G_{xy} = 5.58$ MPa are 1.88, 2.11 and 2.5 times higher than that of the straight sided hole for scarf angles 7°, 5° and 3°, respectively. This demonstrates that scarfing the composite could elevate strains by almost 2.5 times. Such phenomenon is illustrated for three types of laminates, i.e. quasi-isotropic, angle-ply and hard laminates, in Figure 9.

Additionally, due to scarfing and therefore imposed anisotropy in the scarfed region, notable out of plane deformation of the scarfed laminate takes place under the action of membrane loading. This is accompanied by bending of the scarfed region about both the $x$ and $y$ axes, as shown in Figure 10 for a typical quasi-isotropic stacking sequence, i.e. [45/-45/90/0]ₛ. As it can be seen from the figure, the lower the scarf angles, the higher the effect of anisotropy induced bending, resulting in greater out of plane deformations. Therefore, for small scarf angles a higher contribution of bending effects can be expected in the determination of the STRCF.

Another interesting observation is that, unlike straight sided holes and depending on the level of anisotropy, the location of maximum strain does not necessarily take place at a 90º angle to the loading direction (for the case of uniaxial loading). Figure 11 demonstrates this for several stacking sequences and a scarf angle of 7º. As shown in Figure 11e, for a hard laminate with lay-up $[0_4]_s$, there is no anisotropy in the scarf region therefore the location of the maximum strain is at a 90º angle to the loading direction. It is worth noting that often the highest SCF belongs to plies that make the least angle with the loading direction, i.e. 0º plies. For quasi-isotropic laminates of $[45/-45/90/0]_s$, $[45/-45/0/90]_s$ and $[45/0/-45/90]_s$ (see Figure 11a-c), the anisotropy shifts the location of the maximum strain to approximately 114º with respect to the loading direction. This is due to fully populated [A], [B] and [D] stiffness matrices in the scarfed region leading to a complex extension, bending and twisting of the scarfed region shifting the location of maximum strain. As shown in Figure 11d, a laminate with stacking sequence of $[0/45/-45/90]_s$ behaves similar to a lay-up $[0_4]_s$ as a result of demonstrating less anisotropy. This clearly demonstrates the impact of stacking sequence and therefore anisotropy not only on strain concentration magnitude but also on the location of the point of maximum strain.

A key reflection on the preceding findings is that typical stacking sequences used in airframe composite components can significantly influence the magnitude of stress/strain concentration factors if the component is subjected to scarf repair resulting from foreign object damage (thickness $\approx$ 1 mm, $\geq$ 20 mm). Currently, stacking sequence rules for airframe structures do not include preference for the performance of the stacking sequence under scarf repair. As shown in the study, stacking sequence will have a prominent role in stress/strain concentration factors. Therefore, developing and considering stacking sequence rules reflecting repair requirements at the initial design phase will be beneficial for the manufacturing, maintenance, repair and overhaul of such structures.

# 6    Concluding remarks

In this paper, a critical assessment of current methodologies to determine stress/strain concentration factors associated with large scarfed holes in composite laminates has demonstrated that existing analytical methods are only appropriate within a constrained hole diameter range. In particular, numerical analysis considering scarfed holes of diameter equal to 20 mm have determined the existing methods to be inaccurate. It was demonstrated that the use of computationally efficient quarter FEMs are not suitable to capture behaviour of scarfed laminated composite structures. Hence, a series of three-dimensional full finite element models were developed to understand the influence of stacking sequence and scarf angle on strain/stress resultant concentrations under uniaxial tensile loading. The generated results have enabled new understanding on the influence of laminate stacking sequence on strain/stress concentration in thin laminates ($\approx$ 1 mm) with large scarf angles and for the first time that strain concentrations are not only dependant on the laminate membrane stiffness but also on laminate bending stiffness, due to the anisotropy created as a result of the scarf angle. The qualitative behaviour of STRCF of scarfed laminates is similar to straight sided holes. In other words, strain distribution from the edge decays exponentially from the edge of the hole/scarf for both straight sided holes and scarfed holes. Furthermore, the higher the homogenised shear modulus of the laminate, the less is the stress/strain concentration value. However, quantitative analysis clearly illustrates that smaller scarf angles lead to higher STRCF magnitudes. Scarfing with low angles is demonstrated to elevate strains by a factor of 2.5 when compared with baseline straight sided holes. Such high strain concentrations combined with imposed strain concentrations arising from manufacturing processes such as machining and milling used for scarfing could reduce the overall static and fatigue strength of the scarfed laminate significantly. Additionally, unlike straight sided holes, peak stresses in scarfed laminates are dependent on the strain distribution in the scarfed region and the stacking sequence of the

laminate, i.e. bending stiffness of the laminate. Moreover, the location of maximum strain does not necessarily occur at 90º to the loading direction (for uniaxial loading) and maximum strain location is again dependent on the level of anisotropy resulting from stacking sequence and scarfing angle.

# Appendix A

Table A-1: A summary of generated stacking sequences and their homogenised mechanical properties

**Stacking sequences**

| | | | | | | | | | | | | | | | | |
|---|---|---|---|---|---|---|---|---|---|---|---|---|---|---|---|---|
| Ply 1 | 0 | 90 | 90 | 90 | 90 | 0 | 0 | 0 | 90 | 90 | 0 | 0 | 0 | 0 | 90 | 90 |
| Ply 2 | 0 | 0 | 90 | 90 | 90 | 90 | 0 | 0 | 0 | 0 | 90 | 90 | 0 | 90 | 0 | 90 |
| Ply 3 | 0 | 0 | 0 | 90 | 90 | 0 | 90 | 0 | 90 | 0 | 90 | 0 | 90 | 90 | 90 | 0 |
| Ply 4 | 0 | 0 | 0 | 0 | 90 | 0 | 0 | 90 | 0 | 90 | 0 | 90 | 90 | 90 | 90 | 90 |
| Ply 5 | 0 | 0 | 0 | 0 | 90 | 0 | 0 | 90 | 0 | 90 | 0 | 90 | 90 | 90 | 90 | 90 |
| Ply 6 | 0 | 0 | 0 | 90 | 90 | 0 | 90 | 0 | 90 | 0 | 90 | 0 | 90 | 90 | 90 | 0 |
| Ply 7 | 0 | 0 | 90 | 90 | 90 | 90 | 0 | 0 | 0 | 0 | 90 | 90 | 0 | 90 | 0 | 90 |
| Ply 8 | 0 | 90 | 90 | 90 | 90 | 0 | 0 | 0 | 90 | 90 | 0 | 0 | 0 | 0 | 90 | 90 |
| Ex (GPa) | 117.33 | 91.10 | 64.30 | 37.43 | 10.54 | 91.10 | 91.10 | 91.10 | 64.30 | 64.30 | 64.30 | 64.30 | 64.30 | 37.43 | 37.43 | 37.43 |
| Ey (GPa) | 10.54 | 37.43 | 64.30 | 91.10 | 117.33 | 37.43 | 37.43 | 37.43 | 64.30 | 64.30 | 64.30 | 64.30 | 64.30 | 91.10 | 91.10 | 91.10 |
| Gxy (GPa) | 5.58 | 5.58 | 5.58 | 5.58 | 5.58 | 5.58 | 5.58 | 5.58 | 5.58 | 5.58 | 5.58 | 5.58 | 5.58 | 5.58 | 5.58 | 5.58 |
| $\upsilon yx$ | 0.30 | 0.08 | 0.05 | 0.03 | 0.03 | 0.08 | 0.08 | 0.08 | 0.05 | 0.05 | 0.05 | 0.05 | 0.05 | 0.03 | 0.03 | 0.03 |
| $\upsilon xy$ | 0.03 | 0.03 | 0.05 | 0.08 | 0.30 | 0.03 | 0.03 | 0.03 | 0.05 | 0.05 | 0.05 | 0.05 | 0.05 | 0.08 | 0.08 | 0.08 |

| | | | | | | | | | | | | | | | | |
|---|---|---|---|---|---|---|---|---|---|---|---|---|---|---|---|---|
| Ply 1 | 15 | 15 | 15 | 30 | 30 | 30 | 45 | 45 | 45 | 60 | 60 | 60 | 75 | 75 | 75 | 15 |
| Ply 2 | -15 | -15 | -15 | -30 | -30 | -30 | -45 | -45 | -45 | -60 | -60 | -60 | -75 | -75 | -75 | -15 |
| Ply 3 | 0 | 90 | 90 | 0 | 90 | 90 | 0 | 90 | 90 | 0 | 90 | 90 | 0 | 90 | 90 | 15 |
| Ply 4 | 0 | 0 | 90 | 0 | 0 | 90 | 0 | 0 | 90 | 0 | 0 | 90 | 0 | 0 | 90 | -15 |
| Ply 5 | 0 | 0 | 90 | 0 | 0 | 90 | 0 | 0 | 90 | 0 | 0 | 90 | 0 | 0 | 90 | -15 |
| Ply 6 | 0 | 90 | 90 | 0 | 90 | 90 | 0 | 90 | 90 | 0 | 90 | 90 | 0 | 90 | 90 | 15 |
| Ply 7 | -15 | -15 | -15 | -30 | -30 | -30 | -45 | -45 | -45 | -60 | -60 | -60 | -75 | -75 | -75 | -15 |
| Ply 8 | 15 | 15 | 15 | 30 | 30 | 30 | 45 | 45 | 45 | 60 | 60 | 60 | 75 | 75 | 75 | 15 |
| Ex (GPa) | 107.95 | 83.59 | 57.11 | 84.66 | 64.72 | 39.30 | 68.98 | 47.18 | 21.89 | 64.72 | 39.30 | 13.03 | 64.24 | 37.55 | 10.75 | 97.10 |
| Ey (GPa) | 10.75 | 37.55 | 64.24 | 13.03 | 39.30 | 64.72 | 21.89 | 47.18 | 68.98 | 39.30 | 64.72 | 84.66 | 57.11 | 83.59 | 107.95 | 10.73 |
| Gxy (GPa) | 8.71 | 8.71 | 8.71 | 14.98 | 14.98 | 14.98 | 18.11 | 18.11 | 18.11 | 14.98 | 14.98 | 14.98 | 8.71 | 8.71 | 8.71 | 11.85 |
| $\upsilon yx$ | 0.57 | 0.17 | 0.10 | 0.86 | 0.30 | 0.18 | 0.63 | 0.30 | 0.20 | 0.30 | 0.18 | 0.13 | 0.11 | 0.07 | 0.06 | 0.82 |
| $\upsilon xy$ | 0.06 | 0.07 | 0.11 | 0.13 | 0.18 | 0.30 | 0.20 | 0.30 | 0.63 | 0.18 | 0.30 | 0.86 | 0.10 | 0.17 | 0.57 | 0.09 |

| | | | | | | | | | | | | | | |
|---|---|---|---|---|---|---|---|---|---|---|---|---|---|---|
| Ply 1 | 30 | 45 | 60 | 75 | 45 | 45 | 45 | 0 | 45 | 45 | 45 | 0 | 0 | 0 |
| Ply 2 | -30 | -45 | -60 | -75 | -45 | -45 | 0 | 45 | -45 | 0 | 0 | 45 | 45 | 0 |
| Ply 3 | 30 | 45 | 60 | 75 | 90 | 0 | -45 | -45 | 0 | -45 | 0 | -45 | 0 | 45 |
| Ply 4 | -30 | -45 | -60 | -75 | 0 | 90 | 90 | 90 | 0 | 0 | -45 | 0 | -45 | -45 |
| Ply 5 | -30 | -45 | -60 | -75 | 0 | 90 | 90 | 90 | 0 | 0 | -45 | 0 | -45 | -45 |
| Ply 6 | 30 | 45 | 60 | 75 | 90 | 0 | -45 | -45 | 0 | -45 | 0 | -45 | 0 | 45 |
| Ply 7 | -30 | -45 | -60 | -75 | -45 | -45 | 0 | 45 | -45 | 0 | 0 | 45 | 45 | 0 |
| Ply 8 | 30 | 45 | 60 | 75 | 45 | 45 | 45 | 0 | 45 | 45 | 45 | 0 | 0 | 0 |
| Ex (GPa) | 46.83 | 19.17 | 11.36 | 10.73 | 47.18 | 47.18 | 47.18 | 47.18 | 68.98 | 68.98 | 68.98 | 68.98 | 68.98 | 68.98 |
| Ey (GPa) | 12.10 | 19.17 | 63.24 | 97.10 | 47.18 | 47.18 | 47.18 | 47.18 | 21.89 | 21.89 | 21.89 | 21.89 | 21.89 | 21.89 |
| Gxy (GPa) | 24.37 | 30.64 | 20.28 | 11.85 | 18.11 | 18.11 | 18.11 | 18.11 | 18.11 | 18.11 | 18.11 | 18.11 | 18.11 | 18.11 |
| $\upsilon yx$ | 1.17 | 0.72 | 0.21 | 0.09 | 0.30 | 0.30 | 0.30 | 0.30 | 0.63 | 0.63 | 0.63 | 0.63 | 0.63 | 0.63 |
| $\upsilon xy$ | 0.30 | 0.72 | 1.18 | 0.82 | 0.30 | 0.30 | 0.30 | 0.30 | 0.20 | 0.20 | 0.20 | 0.20 | 0.20 | 0.20 |

## 7   References

1.   Yang C, Tomblin JS, Salah L. Stress model and strain energy release rate of a prescribed crack in scarf joint/repair of composite panels. J Compos Mater [Internet]. 2015;49(29):3635–63. Available from: http://dx.doi.org/10.1177/0021998314568326

2.   Niedernhuber M, Holtmannspötter J, Ehrlich I. Fiber-oriented repair geometries for composite materials. Vol. 94, Composites Part B: Engineering. 2016. p. 327–37.

3.   Wang CH, Duong CN. Bonded Joints and Repairs to Composite Airframe Structures. Bonded Joints and Repairs to Composite Airframe Structures. 2015. 1-295 p.

4.   Ueda M, Miyake S, Hasegawa H, Hirano Y. Instantaneous mechanical fastening of quasi-isotropic CFRP laminates by a self-piercing rivet. Compos Struct. 2012;94(11):3388–93.

5.   Gerhard T, Friedrich C. Mechanical fastening of carbon composite tubes, numerical calculation of axial loading capacity and experimental verification. Compos Part B Eng. 2014;67:391–9.

6.   Soutis C, Duan DM, Goutas P. Compressive behaviour of CFRP laminates repaired with adhesively bonded external patches. Compos Struct. 1999;45(4):289–301.

7.   Campilho RDSG, De Moura MFSF, Domingues JJMS, Moura MFSFDE, Domingues JJMS. Stress and failure analyses of scarf repaired CFRP laminates using a cohesive damage model. J Adhes Sci Technol [Internet]. 2007;21(9):855–70. Available from: http://openurl.ingenta.com/content/xref?genre=article&issn=0169-4243&volume=21&issue=9&spage=855

8.   Kweon JH, Jung JW, Kim TH, Choi JH, Kim DH. Failure of carbon composite-to-aluminum joints with combined mechanical fastening and adhesive bonding. Compos

Struct. 2006;75(1–4):192–8.

9.    Boisse P. Advances in composites manufacturing and process design. Advances in
      Composites Manufacturing and Process Design. 2015.

10.   Katnam KB, Da Silva LFM, Young TM. Bonded repair of composite aircraft structures:
      A review of scientific challenges and opportunities [Internet]. Vol. 61, Progress in
      Aerospace    Sciences.    2013.    p.    26–42.    Available    from:    http://ac.els-
      cdn.com/S0376042113000183/1-s2.0-S0376042113000183-main.pdf?_tid=aeabb794-
      12d6-11e7-bc9c-
      00000aacb35d&acdnat=1490610072_4690697fbe9b37e96cf9cd1723021b49

11.   Errouane H, Sereir Z, Chateauneuf A. Numerical model for optimal design of composite
      patch repair of cracked aluminum plates under tension. Int J Adhes Adhes. 2014;49:64–
      72.

12.   Saleem M, Toubal L, Zitoune R, Bougherara H. Investigating the effect of machining
      processes on the mechanical behavior of composite plates with circular holes. Compos
      Part A Appl Sci Manuf. 2013;

13.   Hejjaji A, Zitoune R, Crouzeix L, Roux S Le, Collombet F. Surface and machining
      induced damage characterization of abrasive water jet milled carbon/epoxy composite
      specimens and their impact on tensile behavior. Wear [Internet]. Elsevier; 2017;376–
      377:1356–64.                         Available                         from:
      https://www.sciencedirect.com/science/article/abs/pii/S0043164817303332

14.   Gunnion AJ, Herszberg I. Parametric study of scarf joints in composite structures.
      Compos Struct. 2006;75(1–4):364–76.

15.   Pinto AMGG, Campilho RDSGSG, De Moura MFSFSF, Mendes IR. Numerical

evaluation of three-dimensional scarf repairs in carbon-epoxy structures. In: International Journal of Adhesion and Adhesives. 2010. p. 329–37.

16. Xiaoquan C, Baig Y, Renwei H, Yujian G, Jikui Z. Study of tensile failure mechanisms in scarf repaired CFRP laminates. Int J Adhes Adhes. 2013;41:177–85.

17. Wang CH, Gunnion AJ. Optimum shapes of scarf repairs. Compos Part A Appl Sci Manuf [Internet]. 2009;40(9):1407–18. Available from: http://www.sciencedirect.com/science/article/pii/S1359835X09000451

18. Perillo G, Jørgensen JK, Cristiano R, Riccio A. A Numerical/Experimental Study on the Impact and CAI Behaviour of Glass Reinforced Compsite Plates. Appl Compos Mater [Internet]. 2018 Apr;25(2):425–47. Available from: https://doi.org/10.1007/s10443-017-9628-2

19. Bendemra H, Compston P, Crothers PJ. Optimisation study of tapered scarf and stepped-lap joints in composite repair patches. Compos Struct. 2015;130:1–8.

20. Wang CH, Gunnion AJ, Orifici AC, Rider A. Residual strength of composite laminates containing scarfed and straight-sided holes. Compos Part A Appl Sci Manuf. 2011;42(12):1951–61.

21. Fotouhi M, Jalalvand M, Wisnom MR. Notch insensitive orientation-dispersed pseudo-ductile thin-ply carbon/glass hybrid laminates. Compos Part A Appl Sci Manuf [Internet]. Elsevier; 2018 Jul 1 [cited 2018 May 14];110:29–44. Available from: https://www.sciencedirect.com/science/article/pii/S1359835X18301519

22. Zitoune R, Crouzeix L, Collombet F, Tamine T, Grunevald Y-H. Behaviour of composite plates with drilled and moulded hole under tensile load. Compos Struct [Internet]. 2011;93(9):2384–91. Available from:

http://www.sciencedirect.com/science/article/pii/S0263822311001115

23. Neuber H. G. N. Savin, Stress Concentration around Holes. XI + 430 S. m. 208 Abb. u. 77 Tafeln. Oxford/London/New York/Paris 1961. Pergamon Press. Preis geb. 84 s. net. ZAMM - Zeitschrift für Angew Math und Mech [Internet]. WILEY-VCH Verlag; 1962;42(6):265–265. Available from: http://doi.wiley.com/10.1002/zamm.19620420618

24. Bonora N, Costanzi M, Marchetti M. On closed form solution for the elastic stress field around holes in orthotropic composite plates under in-plane stress conditions. Compos Struct [Internet]. 1993;25(1–4):139–56. Available from: http://linkinghub.elsevier.com/retrieve/pii/026382239390160R

25. Chauhan MM, Sharma DS. Stresses in finite anisotropic plate weakened by rectangular hole. Int J Mech Sci [Internet]. 2015;101–102:272–9. Available from: http://linkinghub.elsevier.com/retrieve/pii/S0020740315002866

26. Makki MM, Chokri B. Experimental, analytical, and finite element study of stress concentration factors for composite materials. J Compos Mater [Internet]. 2017;51(11):1583–94. Available from: http://dx.doi.org/10.1177/0021998316659915

27. Sharma DS. Moment distribution around polygonal holes in infinite plate. Int J Mech Sci. 2014;78:177–82.

28. Darwish F, Tashtoush G, Gharaibeh M. Stress concentration analysis for countersunk rivet holes in orthotropic plates. Eur J Mech A/Solids. 2013;37:69–78.

29. Darwish F, Gharaibeh M, Tashtoush G. A modified equation for the stress concentration factor in countersunk holes. Eur J Mech A/Solids. 2012;36:94–103.

30. Haque A, Ahmed L, Ramasetty A. Stress concentrations and notch sensitivity in woven ceramic matrix composites containing a circular hole-an experimental, analytical, and finite element study. J Am Ceram Soc [Internet]. 2005;88(8):2195–201. Available from: https://ceramics.onlinelibrary.wiley.com/doi/full/10.1111/j.1551-2916.2005.00404.x

31. Hufenbach W, Grüber B, Gottwald R, Lepper M, Zhou B. Analytical and experimental analysis of stress concentration in notched multilayered composites with finite outer boundaries. Mech Compos Mater [Internet]. 2010 Dec;46(5):531–8. Available from: https://doi.org/10.1007/s11029-010-9169-3

32. Grüber B, Gottwald R, Gude M, Lepper M, Modler N, Zhou B. Experimental Strain Measurement for Fibre-Reinforced Finite Mulitlayered Composites with Cut-out Under Bending for Validating an Analytical Calculation Model. Exp Tech [Internet]. 2019;43(2):149–59. Available from: https://doi.org/10.1007/s40799-018-0275-9

33. Khechai A, Tati A, Guettala A. Finite element analysis of stress concentrations and failure criteria in composite plates with circular holes. Front Mech Eng. 2014;9(3):281–94.

34. Toubal L, Karama M, Lorrain B. Stress concentration in a circular hole in composite plate. Compos Struct [Internet]. 2005;68(1):31–6. Available from: https://www.sciencedirect.com/science/article/pii/S0263822304000522

**Tables**

Table 1: Mechanical properties of composite ply

| Material | $h$ (mm) | $E_{11}$ (MPa) | $E_{22}$ (MPa) | $E_{33}$ (MPa) | $\upsilon_{12}$ | $\upsilon_{13}$ | $\upsilon_{23}$ * | $G_{12}$ (MPa) | $G_{13}$ (MPa) | $G_{23}$ * (MPa) |
|---|---|---|---|---|---|---|---|---|---|---|
| Hexcel 8552 AS4 unidirectional prepreg at 190 gsm | 0.187 | 117333.0 | 10544.5 | 10544.5 | 0.3 | 0.3 | 0.49 | 5582.3 | 5582.3 | 3538.2 |

*assumed values

**Figures**
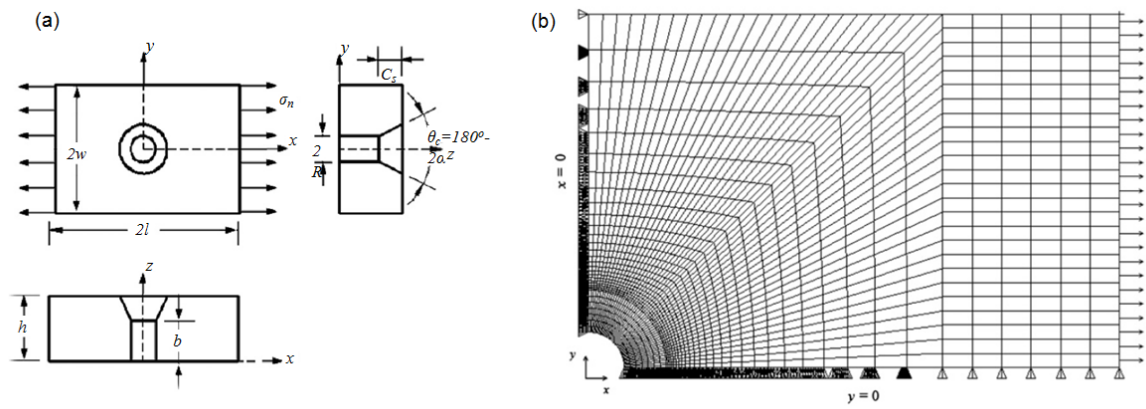


Figure 1: Configuration of (a) countersunk hole and (b) a quarter FEM (28)
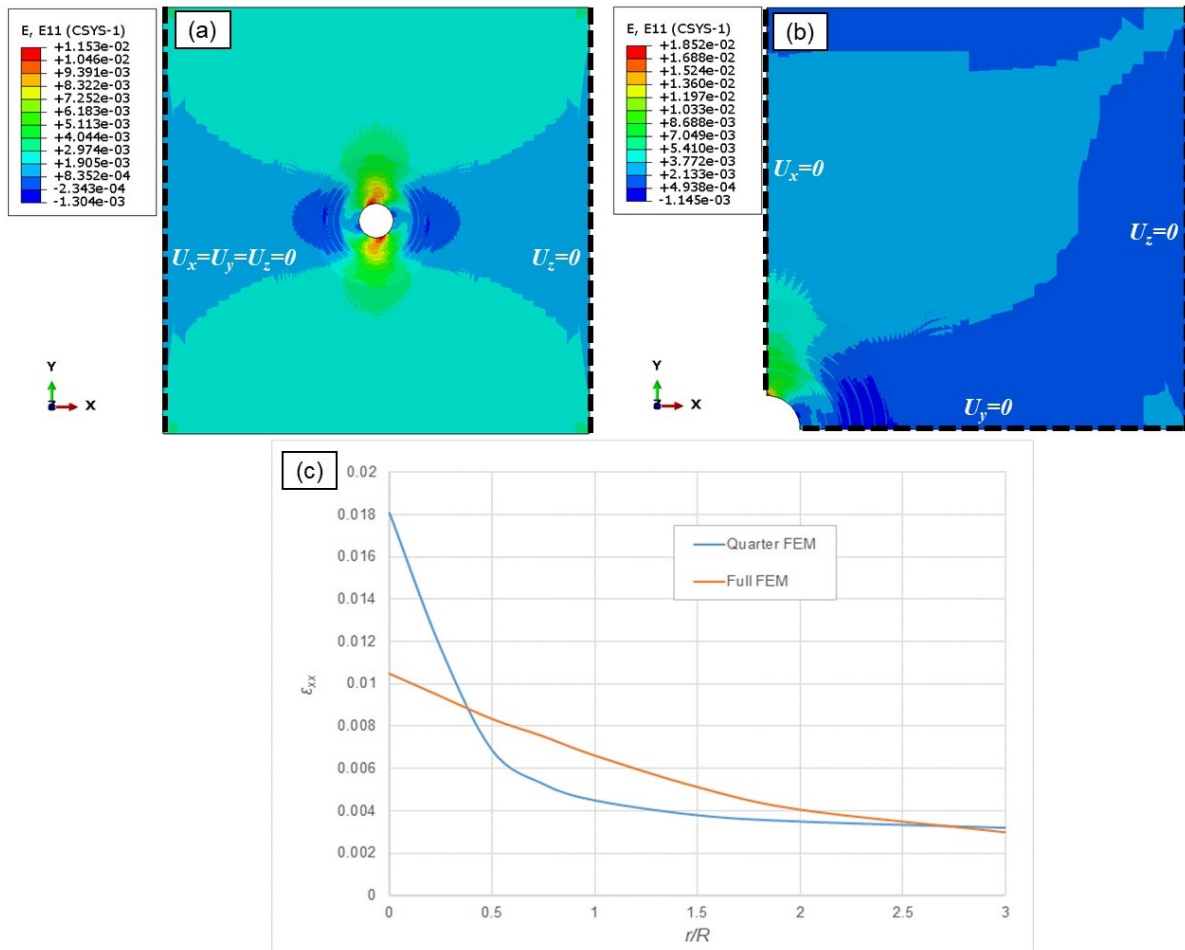
Figure 2: Strain ($\varepsilon_{xx}$) contour plot and boundary conditions of; (a) full scarf FEM; (b) a quarter scarf FEM; (c) strain ($\varepsilon_{xx}$) plots along the line of symmetry for both models for stacking sequence $[45/-45/90/0]_s$
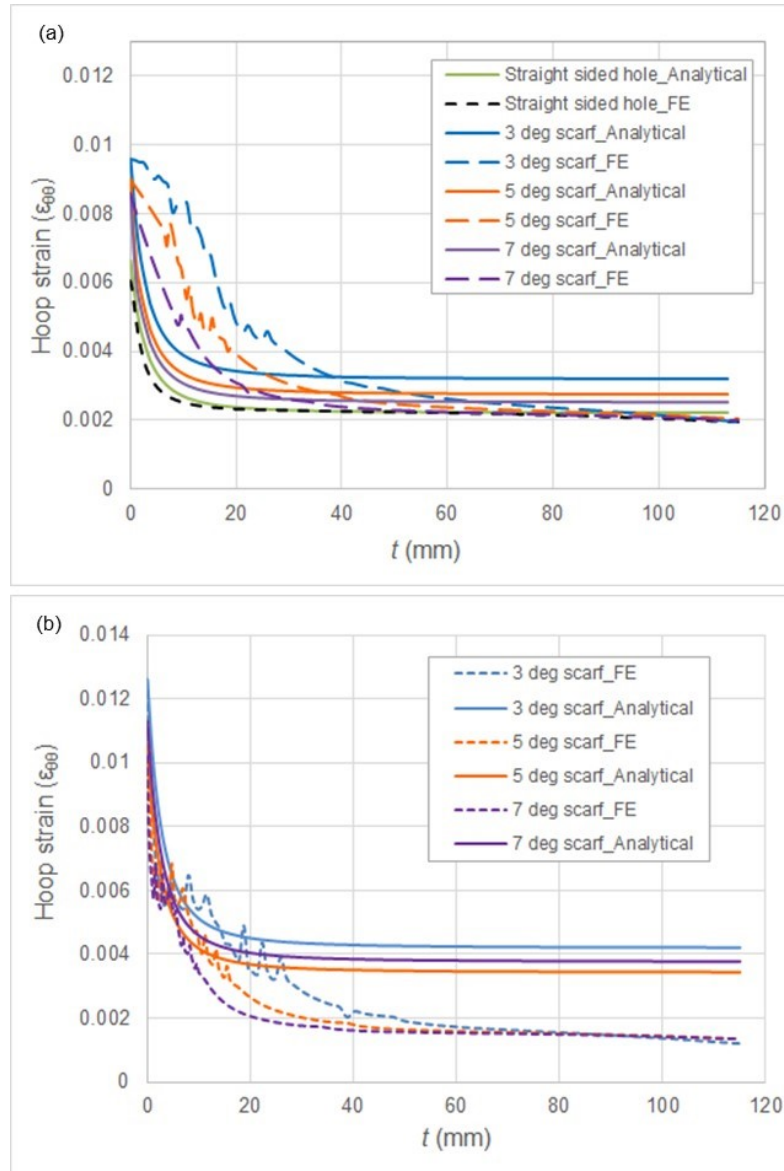
Figure 3: Hoop strain distribution vs the distance from the edge of the hole for scarf angle of 3°, 5° , 7° and straight sided hole with stacking sequences; (a) quasi-isotropic laminate of [45/-45/90/0]$_s$, (b) hard laminate of [0/45/-45/0]$_s$
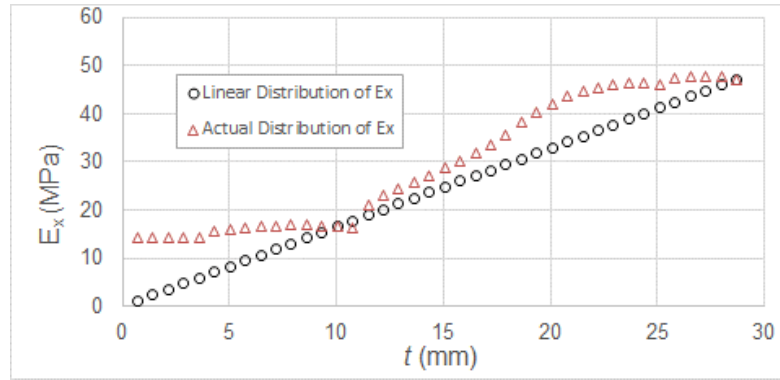
Figure 4: Distribution of homogenised modulus of elasticity in load bearing direction, $E_x$, in the scarf region for scarf angle of 3° and stacking sequence [45/-45/90/0]$_s$
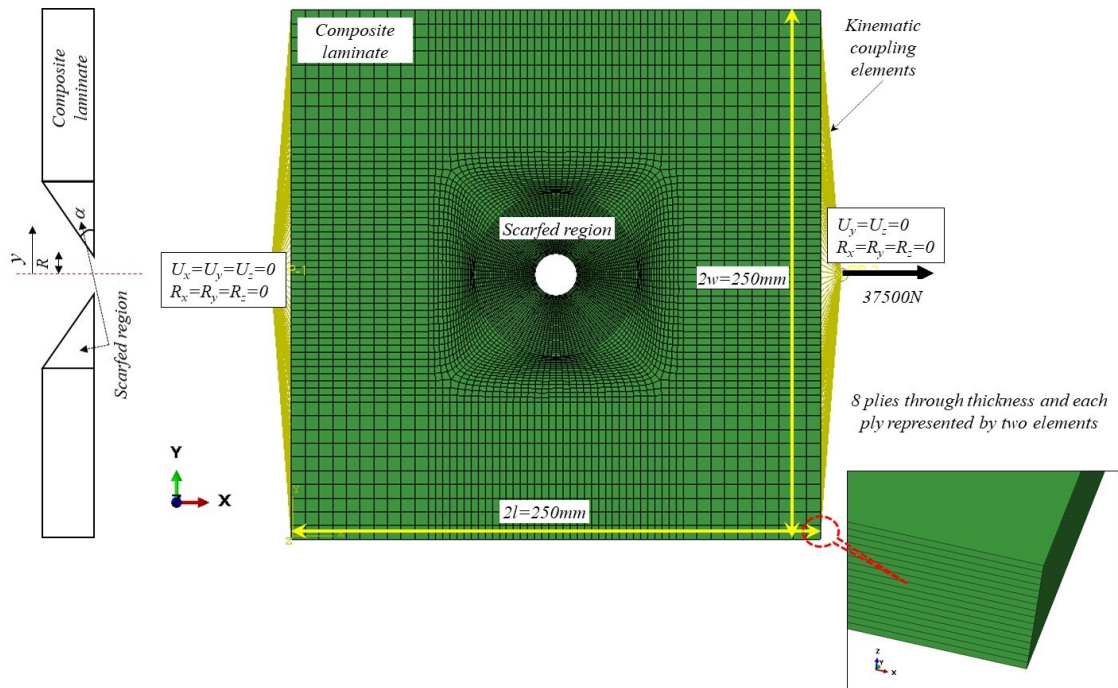
Figure 5: Representation of the scarfed composite structure (scarf angle of 3°) for FEA
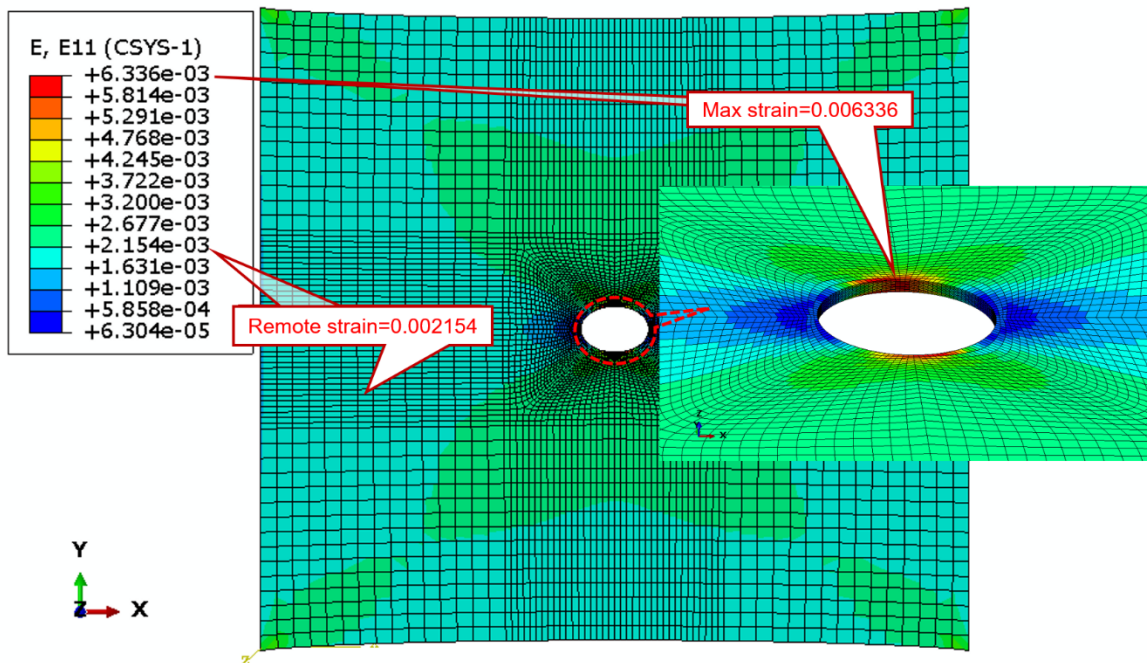


Figure 6: Contour plots of strains in $x$ direction ($\varepsilon_{xx}$) for straight sided hole and

stacking sequence of [45/-45/0/90]$_s$
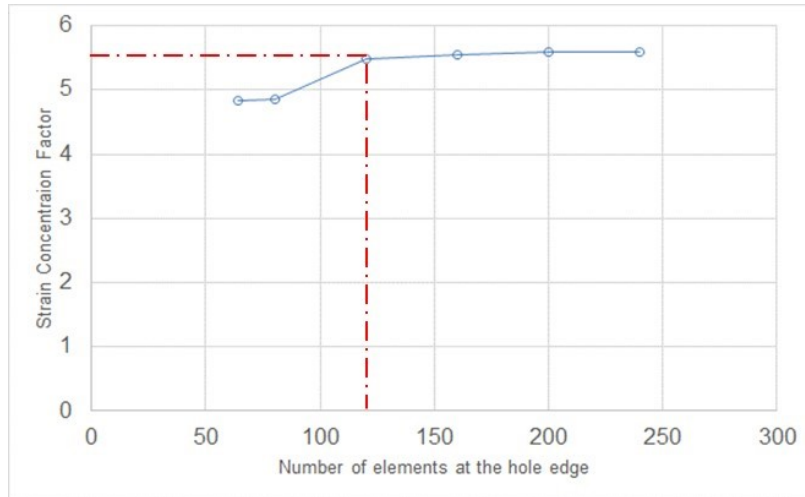
Figure 7: Graph of mesh sensitivity study for scarf angle of 3° and stacking sequence
[45/-45/90/0]$_s$

(a)

(b)

(c)
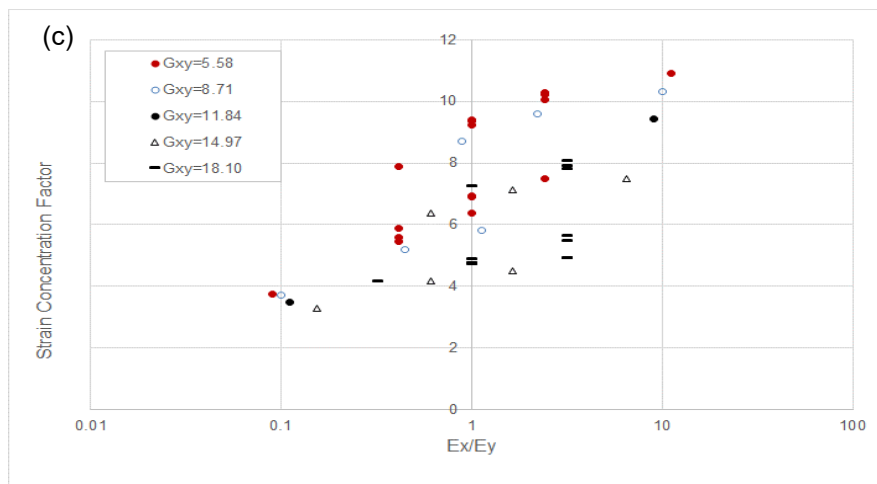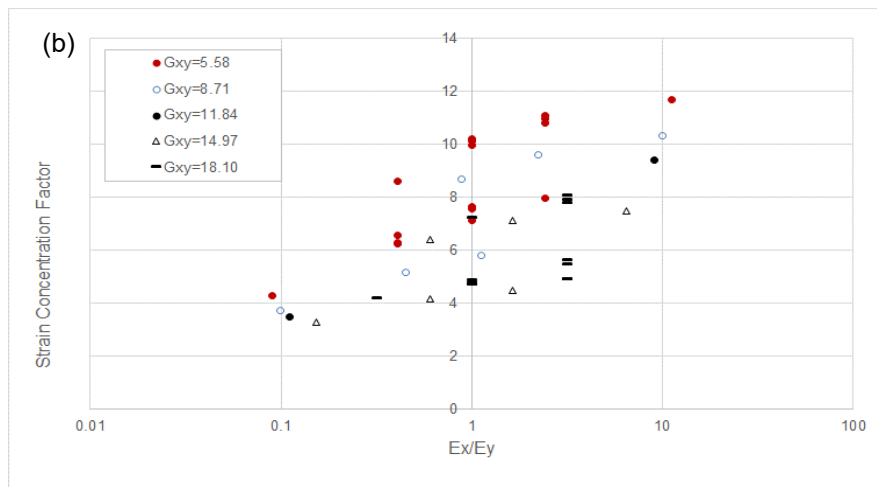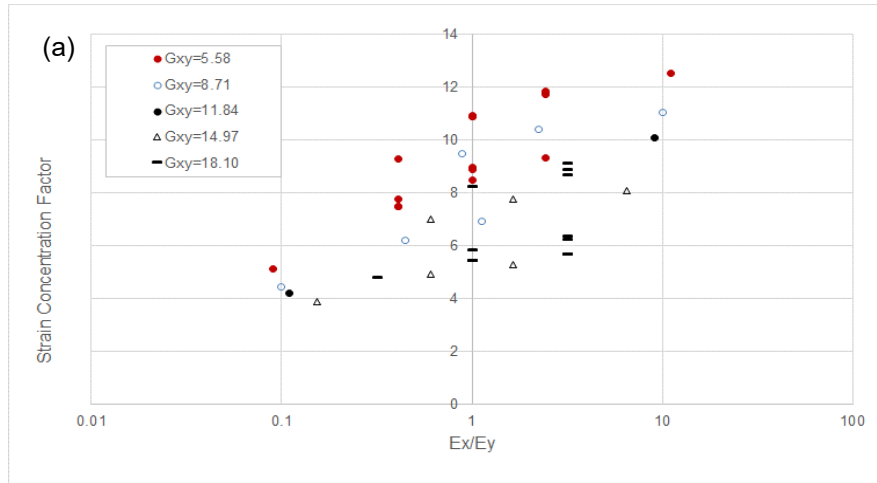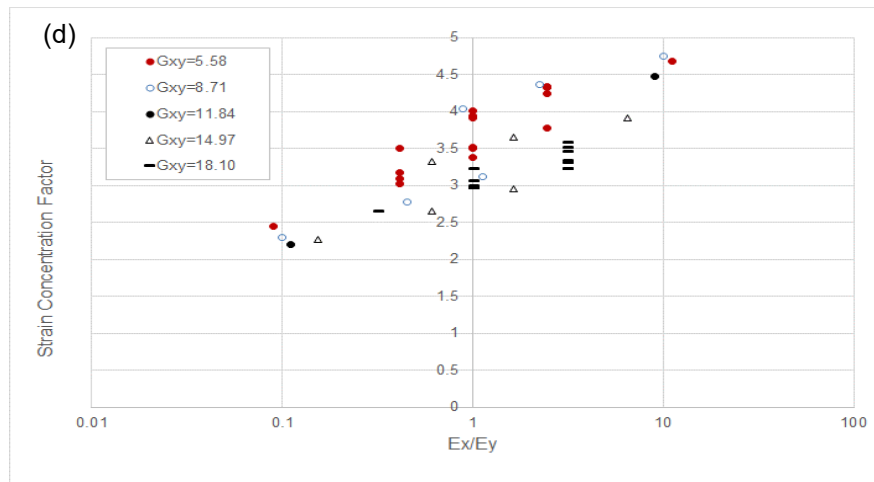
Figure 8: Semi-logarithmic plots of STRCF versus ratio of homogenised modulus of elasticity for various homogenised shear modulus and scarf angles (a) 3º, (b) 5º, (c) 7º and (d) straight sided hole (unit of stiffness is in MPa)
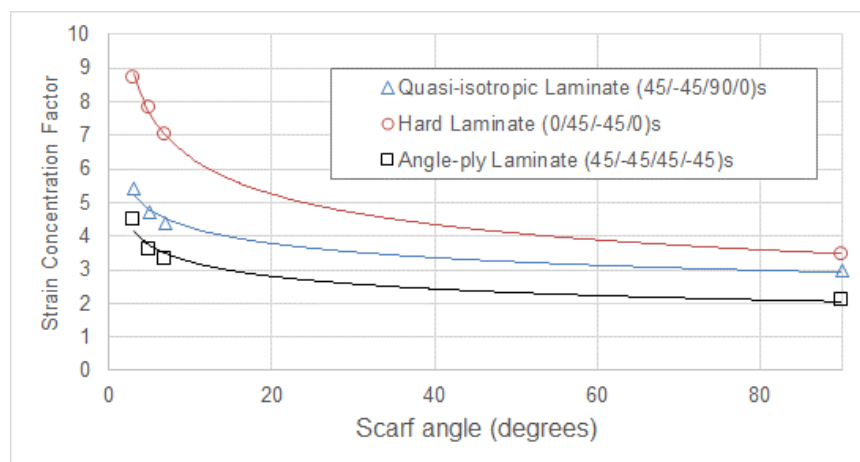


Figure 9: Plot of strain concentration against scarf angle for three types of laminates, i.e. Quasi-isotropic, angle-ply and hard laminates.
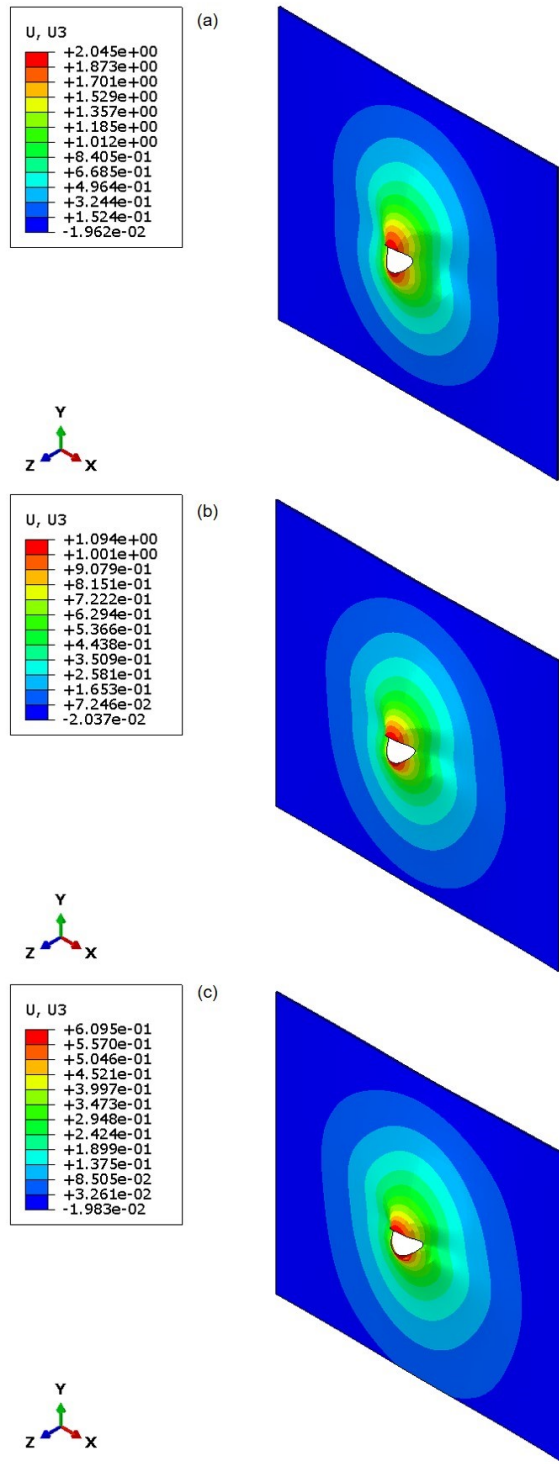
Figure 10: Out of plane deformation of scarfed laminates for scarf angles (a) 3º, (b) 5º and (c) 7º (loading is in direction of $x$ axis and all dimensions are in millimetres)
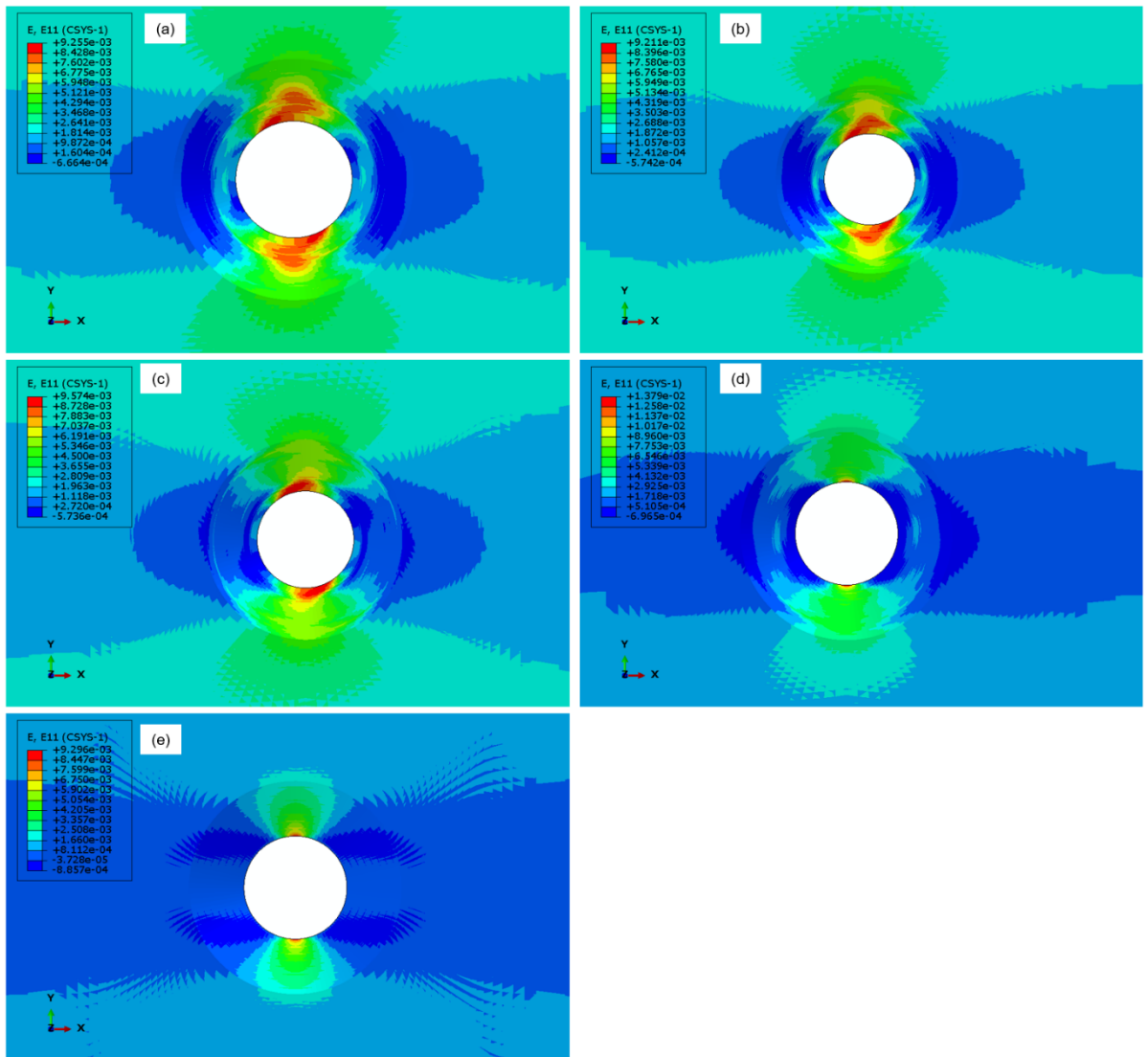
Figure 11: Strain in loading direction for scarf angle of 7° and stacking sequences (a) [45/-45/90/0]$_s$, (b) [45/-45/0/90]$_s$ , (c) [45/0/-45/90]$_s$ , (d) [0/45/-45/90]$_s$ and (e) [0$_4$]$_s$ (loading is in direction of $x$ axis)